20th Australasian Fluid Mechanics Conference
Perth, Australia
5-8 December 2016

Impact of Two Vortex Rings with an Inclined Solid Surface

K. Bourne[1], S. Wahono[1], M. Giacobello[1] and A. Ooi[2]

[1]Aerospace Division
Defence Science and Technology Group, Melbourne 3207, Australia

[2]Department of Mechanical Engineering
University of Melbourne, Parkville, Melbourne 3000, Australia

Abstract

This study numerically investigates the interaction between multiple thin vortex rings and an inclined solid surface at Reynolds numbers of 585 and 1170. The flow mechanics can be considered partially representative of a helicopter rotor in ground effect. Although a significant simplification to the helicopter downwash, vortex ring interactional dynamics provide insight into the fundamental flow features that underlie the complex flow field.

Introduction

The study of vortex rings represents a field of research which has its genesis in the works of Reynolds [17] and Rogers [18]. Since then, there has been a significant amount of theoretical and experimental analysis undertaken, which is well captured in the reviews of Shariff and Leonard [20], Lim and Nickels [12] and Meleshko [14]. Of particular interest to this study are the interactional dynamics between thin vortex rings and solid surfaces, as the flow mechanics can be considered representative of a helicopter rotor wake impinging on the ground.

The interaction between laminar vortex rings and orthogonal solid surfaces is well studied and results in several relatively complicated flow phenomena [19]. With sufficiently high Reynolds numbers (Re) the response as a vortex ring approaches a no-slip wall includes vortex stretching, unsteady separation in the boundary layer flow, formation of a secondary ring, rebound of the primary vortex ring, and subsequent interaction between the primary and secondary vortex rings. Experimental and numerical studies investigating the flow behaviour of isolated vortex rings impacting a no-slip wall with trajectories normal to the wall include [1,3,4,16,23], and reviews are provided by [11, 22].

The available literature relating to oblique interactions between vortex rings and no-slip surfaces is more limited. The experimental work of Lim [10] focused on the role of the no-slip boundary in the formation of bi-helical vortex lines, with Liu [13] undertaking a numerical investigation of the same test conditions. The work of Orlandi and Verzicco [16] used a numerical approach to gain a greater insight into the phenomena observed experimentally by Walker et al [23]. The more recent study of Cheng et al. [3] provides a systematic numerical analysis of an isolated vortex ring impacting a flat wall across a range of angles of incidence and Reynolds numbers.

For the case of multiple vortex rings impacting a wall, the work of Ghosh and Baeder [8] is one of the few examples available in literature. The study sought to numerically investigate two types of multi-vortex behaviour. The first was the phenomenon known as “leapfrogging” [2], which occurs between co-rotating vortex rings in free space, and the second was the orthogonal interaction of multiple vortex rings with a wall.

This numerical study seeks to investigate the case of multiple vortex rings impacting an inclined solid surface, with a focus on the interaction between large-scale flow structures post-impact. Of particular interest are flow structures that are likely to agitate ground-based particles, which can lead to a phenomenon known as brownout. Brownout is a complex aerodynamic environment characterised by entrainment of small ground particles through the helicopter rotor. When brownout conditions are fully developed, cockpit visibility can be wholly obscured.

Numerical Model

Governing Equations and Numerical Approach

The investigation was undertaken using the open source Computational Fluid Dynamics software OpenFOAM [15]. The full Navier–Stokes equations for incompressible flows were solved in the computational domain, which consists of the conservation of mass,

$$\nabla.\mathbf{u} = 0 \tag{1}$$

and the conservation of momentum,

$$\frac{\partial \mathbf{u}}{\partial t} + \nabla.(\mathbf{uu}) = -\frac{1}{\rho}\nabla p + \nabla.2\,\upsilon\,\mathbf{D} + \mathbf{F} \tag{2}$$

where the divergence $\mathbf{C} = \nabla.(\mathbf{uu})$ is the convective term, $\mathbf{P} = -(1/\rho)\nabla p$ is the pressure gradient term, $\mathbf{D} = -0.5(\nabla\mathbf{u} + \nabla\mathbf{u}^T)$ is the rate-of-strain tensor, υ is the kinematic viscosity, and $\mathbf{F}$ is the explicit body force term. The divergence of the rate-of-strain tensor $(\nabla.2\upsilon\mathbf{D})$ is also known as the viscous diffusion term. Taking the divergence from both sides of equation (2) leads to the Poisson equation for pressure,

$$\nabla^2 p = -\nabla.\mathbf{C} \tag{3}$$

The system of Partial Differential Equations (PDE) is solved using the standard Pressure Implicit with Splitting of Operator (PISO) algorithm [7] available in the standard OpenFOAM distribution. The flow simulation is advanced in time using the implicit second order accurate backward differencing scheme. The time increment is chosen to maintain the Courant number below unity during the simulation. The Finite Volume Method (FVM) is used to spatially discretize the convective and diffusive terms in the governing equations. Using this method, the solution domain is divided into a set of discrete volumes (or cell) δVi which fills the entire domain without overlap. Solutions to the governing equations are then sought for each of these discrete volumes at each time step. Using the FVM, the linearized convective term is discretised using Gauss divergence theorem as follows:

$$\nabla.(\mathbf{uu}) = \sum_f \varphi_f\,\mathbf{u}_f \tag{4}$$

where $\varphi_f = \mathbf{u}_f . \mathbf{S}$ is the convective flux through each control volume bounding face *f*, and **S** is the face area normal vector. The convective flux term is evaluated explicitly based on the solution at the current time step. The central differencing scheme is used to interpolate the cell-centred velocity to the face centre. The diffusive terms in both the momentum and Poisson equations can be expressed as a divergence of a gradient term which expands out to a second order Laplacian term. For example, the simplified viscous diffusion term can be discretised using the Gauss divergence term theorem as follows:

$$\upsilon \nabla^2 \mathbf{u} = \sum_f \upsilon \mathbf{S}.(\nabla \mathbf{u})_f \quad (5)$$

where the term $\mathbf{S}.(\nabla \mathbf{u})_f$ is called the diffusive flux and is evaluated based on the velocity gradient at each face. The central differencing scheme is again used to interpolate the velocity gradient evaluated at the cell centres to the face centre. Using the FVM, the discretised equations, including the time derivative, are assembled into a linear system of equations, which can be described in a matrix form as **[A].u = B**, where matrix [**A**] is a sparse block matrix containing the set of coefficients arising from the discretization process, vector **u** is the solution vector, and vector **B** contains the pressure gradient term, body force term and the boundary conditions. This linearized system of equations is solved for a set of boundary conditions using the Preconditioned Bi-Conjugate Gradient Method (PBiCG) [7]. A Diagonal Incomplete L-U decomposition method is used to precondition matrix [**A**] to minimize computational cost. The coupling between the momentum and pressure equations are solved using a segregated approach employed in the PISO algorithm.

Vortex Ring Initialisation

The vortex ring is initialized in the flow field by introducing a time-dependent body force term **F** in equation (2) at the start of the simulation. A vortex ring model based on the equations developed by Sullivan et al. [21] has been used in this study. Sullivan et al. develop their vortex ring model based on experimental parameters and the so-called "slug model". The slug model, as described by Didden [6], assumes a cylindrical "slug" of fluid is ejected from a vortex generator with a velocity u_0 at the exit, which then rolls up to form a vortex ring. The flux of vorticity at the nozzle forms the basis for the slug model.

The experiment parameters used by Sullivan et al. to determine vortex characteristics are based on a piston-nozzle arrangement and require the definition of the piston stroke length and stroke time, L_{piston} and T_{piston} respectively, as well as the radius of the nozzle, $R_{nozzle.}$. From these inputs Sullivan et al. define the radius and circulation of the vortex ring, yielding the following relationship for ejection impulse from the piston:

$$P = \rho \Gamma \pi R_{vortex}^2 . \quad (6)$$

The momentum source term **F** is derived based on the ejection impulse **P** per unit control volume and is implemented in a predefined cylindrical region of radius R_{nozzle}, which has a thickness of one cell. This zone is called the vortex initialization region, and represents the local region over which the momentum source is applied. The model assumes that the momentum imparted to the fluid by the piston movement is approximately equal to the impulse of the ring. The piston movement is modelled incrementally based on the simulation time step:

$$\Delta L_{piston} = U_{piston} \times \Delta t \quad (7)$$

where ΔL_{piston} refers to the incremental movement of the virtual piston, and Δt is the simulation time step. The incremental value of L_{piston} is then used to calculate the radius of the vortex ring and then the vortex ring circulation. Thus, the momentum source F during the formation of the vortex ring is given as:

$$F = \sum_i \frac{1}{\delta V_i} \left(\rho_i \, \Delta\Gamma \, \pi \, \Delta R_{vortex}^2 \right) . \hat{\mathbf{x}} \, , \quad (8)$$

where the subscript i represents the index of the cells included in the vortex ring initialization region, $\hat{x}$ is a unit vector in the direction of the vortex ring travel, and the symbol Δ indicates the cumulative result based on the current simulation time step. The source term F ceases to exist when $\Delta L_{piston} = L_{piston}$ and $\Delta t = T$. The use of a momentum source to establish the vortex ring proves a suitable technique for vortex ring initialization, ostensibly negating the requirement for direct modelling of a vortex generator. Furthermore, the technique offers the benefit of allowing the physics involved in the vortex ring formation to be captured when solving the governing equations.

In order to account for the differing mesh geometries arising from inclination of the wall plane, the initial conditions were set to the point at which the vortex centre point was $2.75R_{vortex}$ from the ground plane. As such, t_0, r_0, u_0 and ω_0 are values for time, vortex radius, velocity and vorticity when the vortex was located $2.75R_{vortex}$ from the ground plane. It should be noted that u_0 represents the initial translational speed of the vortex ring. Test cases were undertaken at Reynolds numbers of 585 and 1180, where Reynolds number is defined as per (9a) based on the vortex ring initial state, and Strouhal number is defined by (9b), where *f* is the vortex ring generation frequency. Dimensionless parameters for time (t_{ND}) and vorticity (ω_{ND}) are defined by (10a) and (10b) respectively.

$$\mathrm{Re} = \frac{2 u_0 r_0}{\upsilon} \quad (a) \qquad St = \frac{f r_0}{u_0} \quad (b) \quad (9)$$

$$t_{ND} = \frac{(t - t_0) u_0}{r_0} \quad (a) \qquad \omega_{ND} = \frac{\omega}{\omega_0} \quad (b) \quad (10)$$

Computational Domain Setup

The computational domain was a rectangular box of size $20R_{vortex} \times 20R_{vortex}$ in the wall-parallel direction, and $15R_{vortex}$ in the wall-normal direction. The domain was meshed using non-uniformly spaced structured hexahedral Cartesian grid. A symmetry boundary condition was applied to all domain boundaries, except the wall boundary which was modelled as a no-slip boundary. Numerical artefacts were not observed at the domain boundaries and analysis of vortex characteristics such as circulation, propagation velocity and vorticity indicated that the domain size was appropriate for the test conditions. The analysis of Cheng et al. [3], Liu [13] and Orlandi and Verzicco [16] also show that the effect of finite domain size is negligible when the domain dimensions are greater than $10R_{vortex}$.

For each test case the vortex rings were initialised at a distance no greater than $5R_{vortex}$ from the wall on a symmetrical mesh with zero skew. The inclined wall was modelled using a second mesh zone, which introduced skew in the axial direction. Analysis of the vortex characteristics as compared to results generated using a straight mesh showed only minor differences in vortex geometry and propagation velocity. As such, the elevated numerical error introduced by the skewed mesh is not deemed significant. The numerical model was validated against experiment data from Chu et al. [4] and Dabiri and Gharib [5].

Results

The second vortex ring was generated at a separation distance equal to the radius of the lead vortex ring, which corresponded to a Strouhal number of 0.48. From the results of Cheng et al. [2] it

was determined that conditions of this study would result in vortex leapfrogging, whereby the trailing vortex (S2) would contract under the influence of the fluid entrainment of the lead vortex (S1) at the same time as the lead vortex is slowed by the induced velocity of the trailing vortex.

If the two vortices are left to develop in quiescent fluid they eventually arrive at sufficiently close proximity to initiate a leapfrog motion, where the trailing vortex moves through the centre of the lead vortex. This study did not seek to investigate leapfrogging flow mechanisms, but focused on the interaction between the two vortex structures and the wall. The separation distance between vortex rings (r_0) ensured the trailing vortex would not leapfrog the lead vortex prior to wall impact. Identical source term parameters were used for both the lead vortex and the trailing vortex ring, and the contraction of the trailing ring under the influence of the lead vortex can be seen in the results.

Re = 585

Presented in figure 1 are composite images of the λ_2 iso-surfaces [9] overlaid with a wall-normal vorticity contour plot for results at Re = 585. The two vortices can be seen on approach to the wall, with the radius of the trailing vortex constrained by the wake of the lead vortex. Also evident is the wake structure of the trailing vortex. When the lead vortex, S1, impacts the inclined wall a secondary vortex is initiated at the high-side (point A). The secondary vortex then progressively develops around the circumference of the lead vortex as the oblique interaction with the wall continues. By the time the primary vortex structure of the lead vortex has impinged upon the wall at the low-side, the secondary structure at the high side has moved around the above the primary structure. The oblique nature of the impact creates variation in the vorticity distribution around the circumference of both primary and secondary vortex structures.

As the trailing vortex, S2, approaches the wall it interacts with the pre-energised boundary layer that persists from the interaction with the lead vortex. Owing to the interaction with the lead vortex wake, the trailing vortex has a smaller diameter and reduced vorticity upon impact with the wall. The trailing vortex does not persist as an individual primary structure; instead it rapidly merges with the primary structure of the lead vortex. The secondary vortex generated by S2 develops outside the merged primary vortex structure and does not directly interact with the secondary vortex of S1. The S1 secondary vortex retains its circumferential asymmetry as it develops, with the high-side of the structure collapsing back toward the ground plane.

Re = 1170

Presented in figure 2 are composite images of the λ_2 iso-surfaces overlaid with a wall-normal vorticity contour plot for Re = 1170. The increase in Reynolds number sees an increase in the azimuthal distribution of vorticity around the circumference of both S1 and S2, and finer scale structures in the wake region. Similar flow mechanisms occur to the Re = 585 test case as the lead vortex impacts the inclined wall. A secondary vortex is asymmetrically generated as the impact of the primary structure progresses, and a tertiary structure also begins to form owing to the increased energy of the impact. As the secondary vortex develops it displays the characteristic "hairpin-like" vortices, a feature which is also reported by Lim, Verzicco and Orlandi and Cheng et al [3, 10, 22].

At the high-side, the impact of the trailing vortex results in ejection of a secondary vortex from the boundary layer. The S2 primary structure quickly coalesces with the primary structure of S1. At the low-side the S2 impact yields a secondary vortex, but a combination of the slope of the wall and proximity to the disintegrating S1 structures means that the S2 structures stay in close proximity to the wall.

Conclusions

For both test cases the interaction of two vortex rings with an inclined wall yields similar flow mechanisms to that of a single vortex. The oblique impact generated asymmetry in both the primary and secondary structures, and there was significant interaction between flow structures at both the high- and low-side impact points. The increase in Reynolds number had the effect of increasing the variation in azimuthal distribution of vorticity. Although a larger number of individual flow structures persisted at Re = 1170, the breakdown of those structures was more rapid and there was increased complexity in the geometry of the flow field near the wall. In both cases the fluctuation of the vortical flow structures represents conditions conducive to the agitation of ground-based particles.

References

[1] Cheng, M., Lou, J. & Lim, T.T., A numerical study of a vortex ring impacting a permeable wall, *Physics of Fluids*, **26**, 2014.

[2] Cheng, M., Lou, J. & Lim, T.T., Leapfrogging of multiple coaxial viscous vortex rings, *Physics of Fluids*, **27**, 2015.

[3] Cheng, M., Lou, J. & Luo, L.S., Numerical Study of a Vortex Ring Impacting a Flat Wall, *J. Fluid Mech.*, **660**, 2010, 430-455.

[4] Chu, C.C., Wang, C.T. & Hsieh, C.S., An Experimental Investigation of Vortex Motions Near Surfaces, *Physics of Fluids*, **5(3)**, 1993, 662-676.

[5] Dabiri, J.O., & Gharib, M., Fluid Entrainment by Isolated Vortex Rings, *J. Fluid Mech.*, **511**, 2004, 311-331.

[6] Didden, N., On the Formation of Vortex Rings: Rolling-Up and Production of Circulation, *Journal of Applied Mechanics Physics (ZAMP)*, **30**, 1979, 101-116.

[7] Ferziger, J.H. & Peric, M., Computational Methods for Fluid Dynamics, Springer, 3rd Edition, 2002.

[8] Ghosh, D. & Baeder, J.D., Numerical simulations of vortex ring interactions with a solid wall, *49th AIAA Aerospace Sciences Meeting*, 2011.

[9] Jeong, J. & Hussain, F., On the Identification of a Vortex, *J. Fluid Mech.*, **285**, 1995, 69-94.

[10] Lim, T.T, An experimental study of a vortex ring interacting with an inclined wall, *Experiments in Fluids*, **7**, 1989, 453-463.

[11] Lim, T.T & Adhikari, D., Vortex Rings and Jets: Recent Developments in Near-Field Dynamics, Springer, 2015.

[12] Lim, T.T & Nickels, T.B., Fluid Vortices, Springer, 1995.

[13] Liu, H.L., Vortex Simulation of Unsteady Shear Flow Induced by a Vortex Ring, *Computers and Fluids*, **31**, 2002, 183-207.

[14] Meleshko, V., Coaxial Axisymmetric Vortex Rings: 150 Years after Helmholtz, *Theoretical Computational Fluid Dynamics*, **24**, 2010.

[15] OpenCFD Ltd, *http://www.openfoam.com*, [Last accessed 27th July 2016].

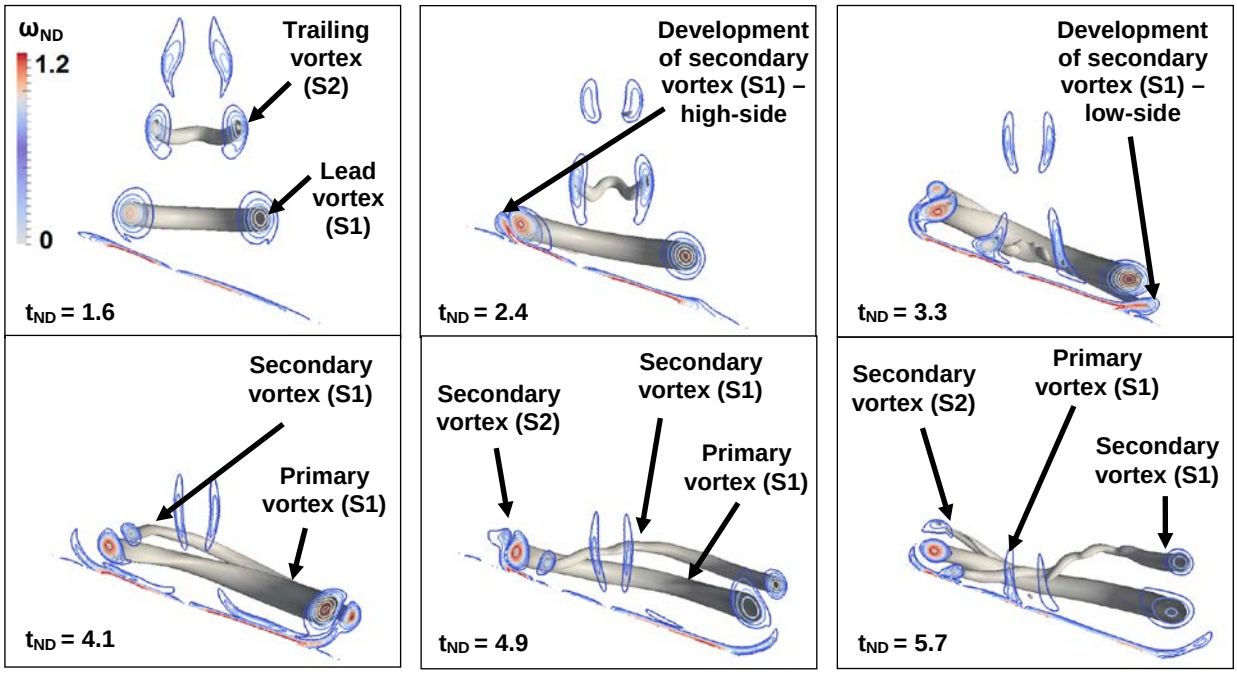

Figure 1. λ_2 iso-surfaces and wall-normal vorticity contour plots for Re = 585.

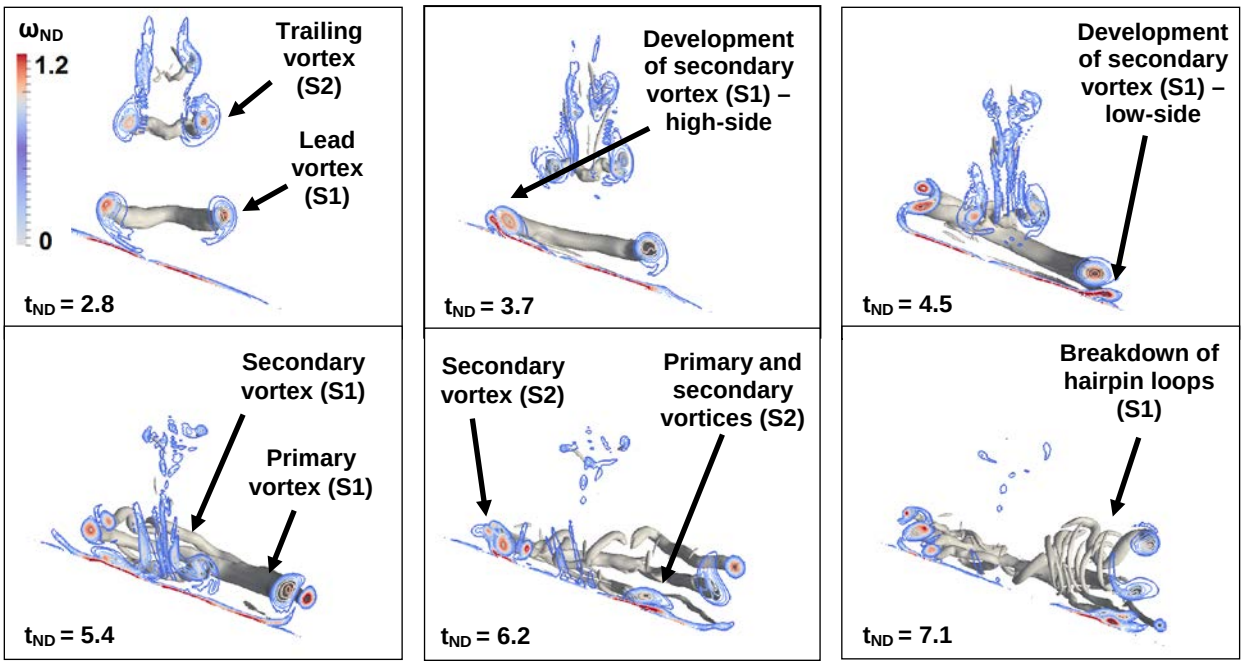

Figure 2. λ_2 iso-surfaces and wall-normal vorticity contour plots for Re = 1170.

[16] Orlandi, P. & Verzicco, R., Vortex Rings Impinging on Walls: Axisymmetric and Three-Dimensional Simulations, *J. Fluid Mech.*, **256**, 1993, 615-646.

[17] Reynolds, O. On the Resistance Encountered by Vortex Rings and the Relation Between Vortex Rings and the Stream-Lines of a Disc, *Nature*, **14**, 1876, 477-479.

[18] Rogers, W.B., On the Formation of Rotating Rings by Air and Liquids under Certain Conditions of Discharge, *American Journal of Science*, **26(2)**, 1858, 246-258.

[19] Saffman, P.G., Vortex Dynamics, Cambridge University Press, 1992.

[20] Shariff, K. & Leonard, K., Vortex Rings, *Annual Review of Fluid Mechanics*, **24**, 1992, 235-279.

[21] Sullivan, I.S, Niemela, J.N., Hershberger, R.E., Bolster, D. & Donnelly, R.J. Dynamics of Thin Vortex Rings, *J. Fluid Mech.*, **609**, 2008, 319-347.

[22] Verzicco, R. & Orlandi, P. Wall/Vortex-Ring Interactions, *Applied Mechanics Review*, **49(10)**, 1996, 447-461

[23] Walker, J.D.A, Smith, C.R., Cerra, A.W., & Doligalski, T.L., The Impact of a Vortex Ring on a Wall. *J. Fluid Mech.*, **181**, 1987, 99-140.